AIAA 81-4017

Electronic Damping of Orthogonal Bending Modes in a Cylindrical Mast—Theory

Charles J. Swigert*
Hughes Aircraft Company, Culver City, Calif.
and
Robert L. Forward†
Hughes Research Laboratories, Malibu, Calif

We present a theoretical model that describes the effect of electronic damping applied to the first two orthogonal bending modes of a cylindrical mast. Computer predictions of the amplitude and phase response of the mast to excitation frequencies around the two closely spaced resonant modes for different levels of feedback damping are obtained. The analytical model predicts that, with only one damping circuit active and low levels of feedback, both modes are weakly damped. However, as the amount of feedback is increased, we find that we can strongly damp one and only one, of the modes. With two orthogonal electronic-damping circuits operating, we can strongly damp both modes. The theoretical predictions of the model agree in detail with the experimental results obtained in the previous paper.

Nomenclature

a_x = elastic coefficient for mast in x direction
a_{xx} = x-x coupling coefficient of i-k loop $= (\hat{x}\cdot\hat{i})(\hat{x}\cdot\hat{k})U_{1x}(z_i)U^*_{1x}(z_k)$
a_{xy} = x-y coupling coefficient of i-k loop $= (\hat{y}\cdot\hat{i})(\hat{x}\cdot\hat{k})U_{1y}(z_i)U^*_{1x}(z_k)$
a_{yx} = y-x coupling coefficient of i-k loop $= (\hat{x}\cdot\hat{i})(\hat{y}\cdot\hat{k})U_{1x}(z_i)U^*_{1y}(z_k)$
a_{yy} = y-y coupling coefficient of i-k loop $= (\hat{y}\cdot\hat{i})(\hat{y}\cdot k)U_{1y}(z_i)U^*_{1y}(z_k)$
b_{xx} = x-x coupling coefficient of j-k loop $= (\hat{x}\cdot\hat{j})(\hat{x}\cdot\hat{l})U_{1x}(z_j)U^*_{1x}(z_l)$
b_{xy} = x-y coupling coefficient of j-l loop $= (\hat{y}\cdot\hat{j})(\hat{x}\cdot\hat{l})U_{1y}(z_j)U^*_{1x}(z_l)$
b_{yx} = y-x coupling coefficient of j-l loop $= (\hat{x}\cdot\hat{j})(\hat{y}\cdot\hat{l})U_{1x}(z_j)U^*_{1y}(z_l)$
b_{yy} = y-y coupling coefficient of j-l loop $= (\hat{y}\cdot\hat{j})(\hat{y}\cdot\hat{l})U_{1y}(z_j)U^*_{1y}(z)$
c_x = x coupling coefficient of m driving array $= (\hat{x}\cdot\hat{m})U^*_{1x}(z_m)$
c_y = y coupling coefficient of m driving array $= (\hat{y}\cdot\hat{m})U^*_{1y}(z_m)$
d_x = damping coefficient for mast in x direction
$f_k(t)$ = forcing function of transducer k
$f_l(t)$ = forcing function of transducer l
$f_m(t)$ = forcing function of driving transducer array m
g_{ik} = gain constant for feedback loop from i to k transducers
g_{jl} = gain constant for feedback loop from j to l transducers
$G_r(s)$ = transfer function to the $\hat{r}$ ray
i = mode number
j = complex variable $= (-1)^{1/2}$
$\hat{i}$ = unit vector in x-y plane in direction of transducer i
$\hat{j}$ = unit vector in x-y plane in direction of transducer j
$\hat{k}$ = unit vector in x-y plane in direction of transducer k
$\hat{l}$ = unit vector in x-y plane in direction of transducer l
$\hat{m}$ = unit vector in x-y plane in direction of driving array m
$\vec{r}$ = arbitrary vector in the x-y plane
$\hat{r}$ = unit vector in the r direction
r_x = component of $\hat{r}$ in the $\hat{x}$ direction $= \hat{r}\cdot\hat{x}$
r_y = component of $\hat{r}$ in the $\hat{y}$ direction $= \hat{r}\cdot\hat{y}$
s = complex Laplace variable $= \sigma + j\omega$
$\vec{u}(z,t)$ = vector transverse displacement of mast at height z
$u_{ix}(t)$ = time function of mode $(2i-1)$ in direction $\hat{x}$
$u_{iy}(t)$ = time function of mode $2i$ in direction $\hat{y}$
$U_{ix}(z)$ = spatial distribution of mode $(2i-1)$ in direction $\hat{x}$
$U_{iy}(z)$ = spatial distribution of mode $2i$ in direction $\hat{y}$
$U^*_{ix}(z)$ = complex conjugate of $U_{ix}(z)$
$U^*_{iy}(z)$ = complex conjugate of $U_{iy}(z)$
$U_x(t)$ = spatial distribution of first mode in $\hat{x}$ direction $= U_{1x}(t)$
$U_y(t)$ = spatial distribution of first mode in $\hat{y}$ direction $= U_{1y}(t)$
$\hat{x}$ = unit vector along one transverse vibrational mode direction
$\hat{y}$ = unit vector along orthogonal transverse vibrational mode direction
$\hat{z}$ = unit vector along axis of mast
z_i = position of transducer i along mast axis
z_j = position of transducer j along mast axis
z_k = position of transducer k along mast axis
z_l = position of transducer l along mast axis
z_m = position of driving array m along mast axis
ω = angular frequency, rad/s
ω_{ix} = eigenfrequency of mode $(2i-1)$ in direction $\hat{x}$
ω_{iy} = eigenfrequency of mode $2i$ in direction $\hat{y}$
ω_x = eigenfrequency of first mode in x direction $= \omega_{1x}$
ω_y = eigenfrequency of first mode in y direction $= \omega_{1y}$
σ = damping, Np/s

Introduction

In a previous paper,[1] electronic damping was applied to the doubly degenerate orthogonal bending modes of a top-loaded mast. The behavior of the two modes of the mast as they interacted with the two electronic damping circuits was quite complex. In this paper we develop a combined electromechanical theoretical model for the mast and the electronic circuits. The predictions of the theoretical model agree in detail with the experimental results. The theoretical model

Received Dec. 12, 1979; revision received Aug. 11, 1980.

*Senior Member of the Technical Staff, Advanced Systems Engineering Department, Tactical Systems Division.

†Senior Scientist, Exploratory Studies Department. Associate Fellow AIAA.

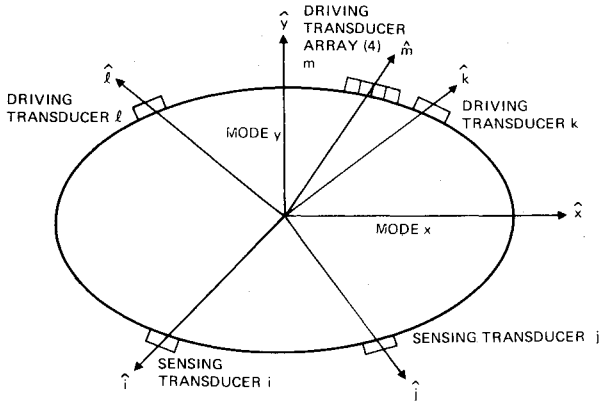

Fig. 1 Top view of cylindrical mast showing labels and relative orientation of mode axes and transducer axes.

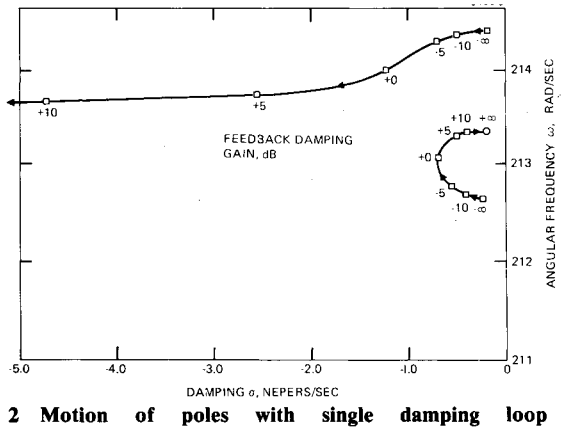

Fig. 2 Motion of poles with single damping loop *j-l* operational—expanded view near mode resonances.

can now be used to predict the performance of electronic damping on similar structures.

Analytical Model

An (x,y,z) coordinate system is chosen with the z axis on the centerline of the mast and the origin at the base of the mast. The $\hat{x}$ and $\hat{y}$ axes are aligned with the orthogonal transverse modes of the mast as shown in Fig. 1, where we have used an exaggerated elliptical cross section for the mast to symbolize the modal direction, although the mast cross section was nearly circular. The feedback transducer axes $\hat{i},\hat{j},\hat{k}$, and $\hat{l}$ are defined by the position of the transducers on the mast, and the driving axis $\hat{m}$ is defined by the position of the driving transducer array.

Analysis

The equation of motion of the mast in the x direction with forces being exerted by transducers k, l, and m is

$$\hat{x}\left[\frac{\partial^2\vec{u}(z,t)\cdot\hat{x}}{\partial t^2}+d_x\frac{\partial\vec{u}\cdot\hat{x}}{\partial t}+a_x\frac{\partial^4\vec{u}\cdot\hat{x}}{\partial z^4}\right]$$
$$=\hat{x}\Big[(\hat{x}\cdot\hat{k})f_k(t)\delta(z-z_k)+(\hat{x}\cdot\hat{l})f_l(t)\delta(z-z_l)$$
$$+(\hat{x}\cdot\hat{m})f_m(t)\delta(z-z_m)\Big] \tag{1}$$

with a similar equation for the y direction.

The equations for the transverse displacement of the mast can be found in standard references such as Morse and Ingard.[2]

$$\vec{u}(z,t)=\sum_i\left[\hat{x}\;\;u_{ix}(t)U_{ix}(z)+\hat{y}\;\;u_{iy}(t)U_{iy}(z)\right] \tag{2}$$

Substituting Eq. (2) into Eq. (1) we obtain

$$\sum_i\left[\frac{\partial^2u_{ix}(t)}{\partial t^2}U_{ix}(z)+d_x\frac{\partial u_{ix}}{\partial t}U_{ix}(z)+a_xu_{ix}(t)\frac{\partial^4U_{ix}(z)}{\partial z^4}\right]$$
$$=(\hat{x}\cdot\hat{k})f_k(t)\delta(z-z_k)+(\hat{x}\cdot\hat{l})f_l(t)\delta(z-z_l)$$
$$+(\hat{x}\cdot\hat{m})f_m(t)\delta(z-z_m) \tag{3}$$

and a similar equation for the y direction.

The eigenfrequencies of each of the modes are determined by the boundary conditions of the mast.[2] Similarly, we can solve for the mode spatial distributions using the boundary conditions and obtain

$$a_x\frac{\partial^4U_{ix}(z)}{\partial z^4}=\omega_{ix}^2U_{ix}(z) \tag{4}$$

with a similar equation for the y direction.

For a long thin mast, the first harmonics are considerably higher in frequency than the two fundamental modes, so for the rest of the analysis we will only include the fundamental mode in the x and y directions (i.e., $i=1$).

If we substitute Eq. (4) into Eq. (3), multiply through by the complex conjugates of the lowest mode in each direction, and integrate both sides while remembering that the spatial mode distributions are orthogonal, we obtain

$$\frac{\partial^2u_{1x}(t)}{\partial t^2}+d_x\frac{\partial u_{1x}(t)}{\partial t}+\omega_{1x}^2u_{1x}(t)=(\hat{x}\cdot\hat{k})f_k(t)U_{1x}^*(z_k)$$
$$+(\hat{x}\cdot\hat{l})f_l(t)U_{1x}^*(z_l)+(\hat{x}\cdot\hat{m})f_m(t)U_{1x}^*(z_m) \tag{5}$$

and a similar equation for the y direction.

We will choose the forcing functions for the k and l drivers to be a gain constant times the rate of change of the mast displacement at the position of the i and j sensing transducers:

$$f_k(t)=-g_{ik}\frac{\partial\vec{u}(z_i,t)\cdot\hat{i}}{\partial t}$$
$$=-g_{ik}\left[(\hat{x}\cdot\hat{i})U_{1x}(z_i)\frac{\partial u_{1x}(t)}{\partial t}+(\hat{y}\cdot\hat{i})U_{1y}(z_i)\frac{\partial u_{1y}(t)}{\partial t}\right] \tag{6a}$$

$$f_l(t)=-g_{jl}\frac{\partial\vec{u}(z_j,t)\cdot\hat{j}}{\partial t}$$
$$=-g_{jl}\left[(\hat{x}\cdot\hat{j})U_{1x}(z_j)\frac{\partial u_{1x}(t)}{\partial t}+(\hat{y}\cdot\hat{j})U_{1y}(z_j)\frac{\partial u_{1y}(t)}{\partial t}\right] \tag{6b}$$

Substituting Eq. (6) into Eq. (5) and rearranging, we obtain

$$\frac{\partial^2u_{1x}(t)}{\partial t^2}+[g_{ik}(\hat{x}\cdot\hat{i})(\hat{x}\cdot\hat{k})U_{1x}(z_i)U_{1x}^*(z_k)$$
$$+g_{jl}(\hat{x}\cdot\hat{j})(\hat{x}\cdot\hat{l})U_{1x}(z_j)U_{1x}^*(z_l)+d_x]\frac{\partial u_{1x}(t)}{\partial t}$$
$$+\omega_{1x}^2u_{1x}(t)+[g_{ik}(\hat{y}\cdot\hat{i})(\hat{x}\cdot\hat{k})U_{1y}(z_i)U_{1x}^*(z_k)$$
$$+g_{jl}(\hat{y}\cdot\hat{j})(\hat{x}\cdot\hat{l})U_{1y}(z_j)U_{1x}^*(z_l)]\frac{\partial u_{1y}(t)}{\partial t}$$
$$=(\hat{x}\cdot\hat{m})U_{1x}^*(z_m)f_m(t) \tag{7}$$

with a similar equation for the y axis. Equation (7) can be further simplified by replacing the products in each term with their equivalent coupling coefficients a_{xx}, a_{xy}..., etc.

Taking the Laplace transform of the simplified expressions for both the x and y directions produces

$$[s^2+(d_x+g_{ik}a_{xx}+g_{jl}b_{xx})s+\omega_x^2]u_x(s)$$
$$+(g_{ik}a_{xy}+g_{jl}b_{xy})su_y(s)=c_xf_m(s) \tag{8a}$$

$$[s^2+(d_y+g_{ik}a_{yy}+g_{jl}b_{yy})s+\omega_y^2]u_y(s)$$
$$+(g_{ik}a_{yx}+g_{jl}b_{yx})su_x(s)=c_yf_m(s) \quad (8b)$$

where in the complex Laplace transform variable $s=\sigma+j\omega$, ω is in rad/s and σ is in Np/s. A neper (Np) is a dimensionless ratio of powers and 1 Np is equal to 8.686 dB. Solving for $u_x(s)$ and $u_y(s)$, we obtain the transfer function from the driver transducer to the mode amplitude

$$G_x(s)=(u_x/f_m)(s)$$
$$=\{c_xs^2+[c_xd_y+g_{ik}(c_xa_{yy}-c_ya_{xy})$$
$$+g_{jl}(c_xb_{yy}-c_yb_{xy})]s+c_x\omega_y^2\}/\Delta(s) \quad (9a)$$

$$G_y(s)=(u_y/f_m)(s)$$
$$=\{c_ys^2+[c_yd_x+g_{ik}(c_ya_{xx}-c_xa_{yx})$$
$$+g_{jl}(c_yb_{xx}-c_xb_{yx})]s+c_y\omega_x^2\}/\Delta(s) \quad (9b)$$

where the denominator of the transfer function is

$$\Delta(s)=[s^2+(d_x+g_{ik}a_{xx}+g_{jl}b_{xx})s+\omega_x^2]$$
$$\times[s^2+(d_y+g_{ik}a_{yy}+g_{jl}b_{yy})s+\omega_y^2]$$
$$-s^2(g_{ik}a_{xy}+g_{jl}b_{xy})(g_{ik}a_{yk}+g_{jl}b_{yx}) \quad (10)$$

As a check of Eq. (9), we see, for no damping (i.e., $d_x=d_y=0$ and $g_{il}=g_{jk}=0$), that

$$G_x(s)=\frac{u_x}{f_m}(s)=\frac{c_x}{s^2+\omega_x^2}$$
$$G_y(s)=\frac{u_y}{f_m}(s)=\frac{c_y}{s^2+\omega_y^2} \quad (11)$$

The interpretation of Eq. (11) is that the driving force $f_m(t)$ can excite both the x and y modes, that are resonant at ω_x and ω_y. The amount of excitation of each mode is determined by the driver coupling constants c_x and c_y.

To generalize the transfer function, we want to determine the excitation on an arbitrary ray in the r direction in the x-y plane due to the forcing function of the m transducer array:

$$u_r(s)\equiv\hat{r}\cdot\vec{U}(s)=(\hat{r}\cdot\hat{x})u_x(s)+(\hat{r}\cdot\hat{y})u_y(s)$$
$$=r_xu_x(s)+r_yu_y(s) \quad (12)$$

The transfer function to the r ray is then

$$G_r(s)=(u_r/f_m)(s)=Z(s)/\Delta(s) \quad (13)$$

where

$$Z(s)=s^2[r_xc_x+r_yc_y]+s[r_xc_xd_y+r_yc_yd_x$$
$$+g_{ik}(r_xc_xa_{yy}-r_xc_ya_{xy}+r_yc_ya_{xx}-r_yc_xa_{yx})$$
$$+g_{jl}(r_xc_xb_{yy}-r_xc_yb_{xy}+r_yc_yb_{xx}-r_yc_xb_{yx})]$$
$$+[r_xc_x\omega_y^2+r_yc_y\omega_x^2] \quad (14)$$

and $\Delta(s)$ is given by Eq. (10).

The transfer function given by Eq. (13) is general enough to give the amplitude and phase of the response of the mast at any point for any position of the driver, any position for each of the four transducers used in the two feedback loops, and any gain level in those feedback damping circuits.

Computer Simulations

The transfer function given by Eq. (13) was then used in two computer programs. One calculated the position of the poles and zeros in the complex plane and their locus in the plane with increasing gain in the two feedback loops. The other program calculated the Bode plots for phase and amplitude response as the driver transducer voltage was swept in frequency across the resonant frequencies of the two modes.

The experimental parameters needed for the initialization of the analytical model are the frequency and damping of the modes, the position of the various transducers, the coupling coefficient of each of the transducers, and the angular orientation of the modes with respect to the transducers. These were obtained from the experimental data reported in Ref. 1.

Single Feedback Damping Loop Analysis

The behavior of the poles and zero for the single feedback damping loop case can perhaps best be understood by a plot of the poles and zeros in the complex plane as a function of increasing gain. As Fig. 2 shows, with no feedback gain (the computer model set -100 dB), there is a pole at $(-0.20, 214.36i)$ and another at $(-0.23, 212.66i)$, with a zero at $(-0.22, 213.34i)$. As the gain in the j-l feedback loop is increased, the zero stays put while both the poles start moving to higher levels of damping. As the gain is increased to around 0 dB, the two poles start to shift toward each other in frequency. At even higher gains the upper pole is increasingly damped, while the lower pole circles back around and returns to a frequency and a Q that are between the values of the original undamped modes. The new high-Q mode can be

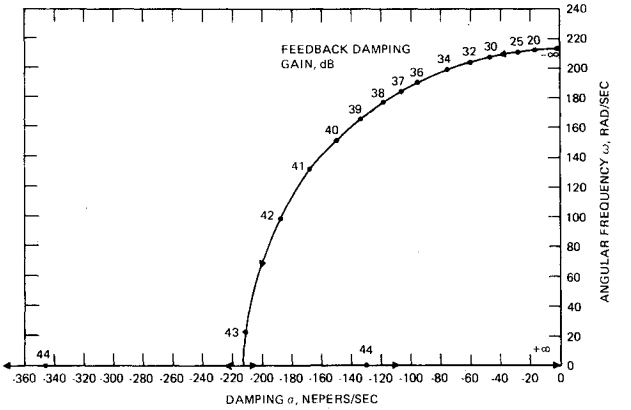

Fig. 3 Motion of damped pole with single damping loop j-l operational.

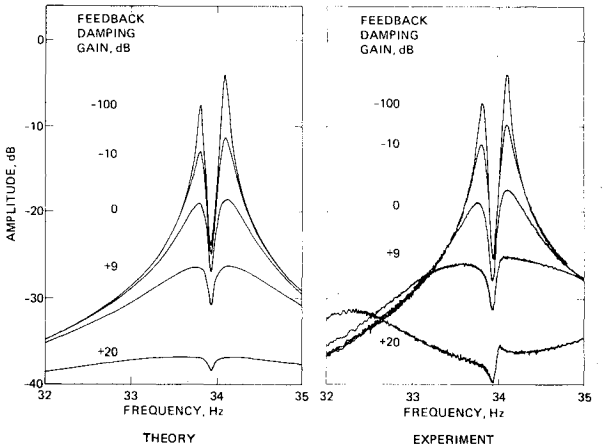

Fig. 4 Amplitude of modes in j-l direction with increasing feedback damping gain in j-l direction.

thought of as a linear superposition of the original modes with the phases adjusted so that the direction of the high-Q mode is orthogonal to the damping loop orientation. The high-Q mode also approaches the zero of the system, so that it will be hard to see in the direction of the transducers that detect the zero.

As the modes reconfigure (or "rotate"), the in-line member of the mode pair is now lined up in the direction of the damping loop and becomes highly damped. The motion of this damped mode in the complex plane is shown in Fig. 3. As the feedback damping gain goes from +15 to +43 dB, the pole moves in a circle whose center is at the origin. It approaches the real axis, where it meets its mate in the negative half of the plane. One of the poles moves out the real axis toward increased damping and the other moves in until it reaches the origin at infinite feedback damping gain.

The map of the poles and zeros in the complex plane does not show the amplitude of coupling. This is seen when we calculate the amplitude of the transfer function to the various transducers. Figure 4 shows the amplitude of the modes seen in the same direction as the feedback damping loop for damping in the j-l direction. The theoretical model shows the higher frequency mode damping faster than the lower mode initially, but for gains higher than 0 dB we are essentially only seeing the damped mode and the zero, since the high-Q mode is hidden by the zero in this direction.

The reason for the +9 dB curve in Fig. 4 is that the experimental data were mistakenly taken at that gain level, and the +9-dB curve and the +10-dB curve are distinctly different. Most of the time, a 1-dB difference in gain would produce a noticeable worsening of the fit between the theoretical model and the experimental data.

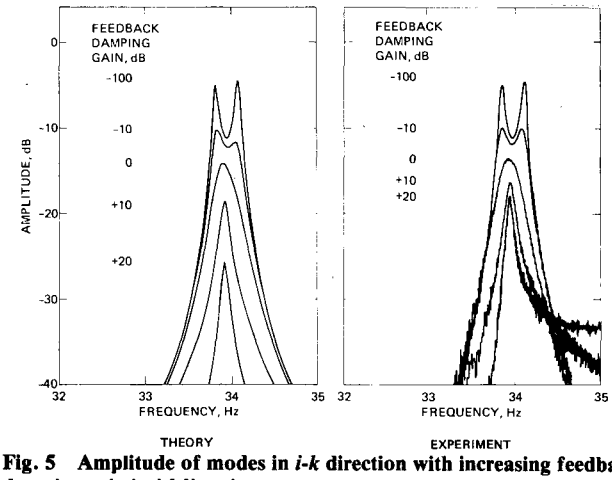

Fig. 5 Amplitude of modes in i-k direction with increasing feedback damping gain in j-l direction.

The theory agrees well with the experimental data, but the agreement becomes poorer at high gain levels. The experimental feedback damping circuit has a 3-Hz-wide bandpass filter centered at 34 Hz to prevent oscillations at higher frequencies. This filter was not included in the theoretical model. This means that the effective gain of the feedback loop was lower outside the bandwidth of the filter. This produced the bulges on either side of the notch in the +20-dB experimental curve.

If we look in the direction orthogonal to the direction of the feedback damping loop, we can then see the high-Q mode develop since there is no zero in this direction to hide it. As Fig. 5 shows, as the feedback gain is increased, the upper frequency mode is damped more rapidly than the lower frequency mode. If we follow the peak of the lower mode, we can see it shift in frequency to a point between the two original mode frequencies. The frequency of the high-Q mode depends on the original orientation of the modes to the transducers. If the original modes were almost lined up on the transducer damping loop axes, then the mode orthogonal to the damping axis would hardly be affected by the single feedback damping circuit. It would move in a small circle, hardly being damped at all, and return to its original Q near its original frequency.

In the theoretical model for this 51 deg orientation, the amplitude of the high-Q peak is decreasing. This is because we chose the driving array to be in the same direction as the feedback damping loop. Thus, as the high-Q mode rotates to be orthogonal to the feedback loop, it is also rotating so that it is orthogonal to the driver, decreasing the coupling. The decrease in amplitude predicted by the model does not agree well with the experimental data. This is because the driving array was not exactly in line with the feedback damping loop, and so retained some residual coupling.

If the i-k damping loop is operated as the single feedback damping circuit instead of the j-l damping loop, then the behavior of the system will be approximately the same, except that the zero, which is only seen in the i-k direction, will also be affected by the feedback gain. This is seen in Fig. 6, which shows the lower pole and the zero moving to higher levels of damping with increased feedback gain, while the upper pole first moves toward higher damping and then returns to a high-Q mode at a frequency between the orthogonal mode frequencies. The damped pole and the zero follow the same circular path that the pole did for the other case, and the motion in the complex plane is identical to that shown in Fig. 3.

When we look at the amplitude plots for the i-k loop single damping orientation, we initially see somewhat the same behavior as before, but now, as shown in Fig. 7, the zero is also damped. Since the zero is moving out of the way of the

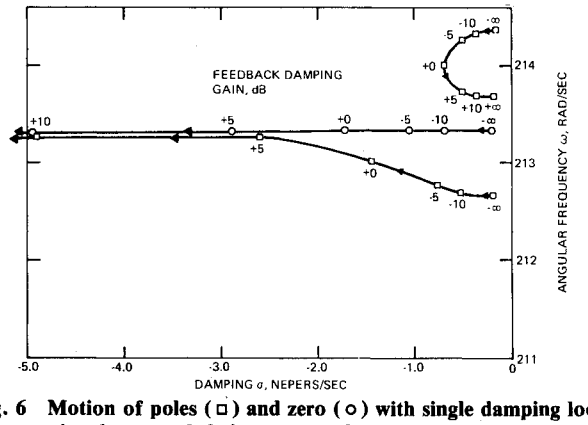

Fig. 6 Motion of poles (□) and zero (○) with single damping loop i-k operational—expanded view near mode resonances.

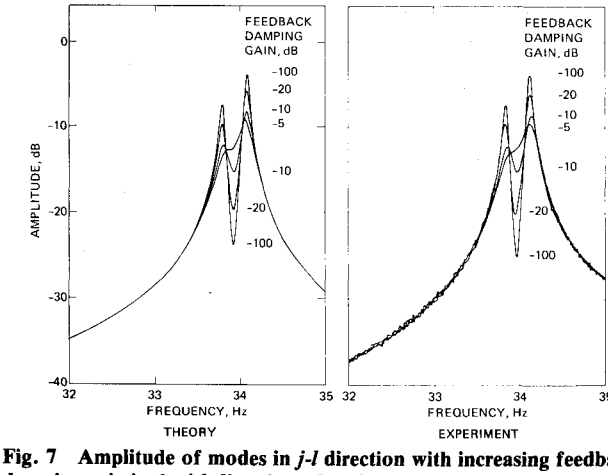

Fig. 7 Amplitude of modes in j-l direction with increasing feedback damping gain in the i-k direction—low feedback damping levels.

high-Q mode, we can see both modes start to shift toward each other in frequency as the feedback gain goes from -20 to -5 dB.

Figure 8 shows what happens to the modes in Fig. 7 as the feedback gain is increased. Notice that at 0 dB there is essentially what looks like a single mode. As the gain is increased, it becomes sharper and shifts lower in frequency, as shown in the pole plot in Fig. 6. Since the feedback damping direction is now orthogonal to both the sensing transducer and the driving transducer, the high-Q mode is rotating toward maximum coupling to both the driver array and the sensing transducer. At effectively infinite gain (+100 dB), the mode Q is back to the mean of the original mode Q's, and the transfer function amplitude is significantly higher than either of the original modes. This theoretical prediction follows well the experimental data to the limit of the gain of the experimental feedback loops (+20 dB).

Figure 9 shows the same damping situation but from the orthogonal direction. These curves are superficially identical to those in Fig. 5, but there are important differences. In Fig. 9, the upper mode is initially less damped than the lower mode, and the upper mode turns into the high-Q mode. The decrease in amplitude of the high-Q mode is identical in the theoretical model for both Figs. 5 and 9, but in Fig. 5 it was due to the high-Q mode rotating away from the driver, whereas in Fig. 9 it is due to the mode rotating away from the sensing transducer. This is more dramatically shown in the experimental curves. In Fig. 5, the amplitude of the high-Q mode did not decrease as fast as the theory, indicating that the driving array was not orthogonal to the feedback loop. In Fig. 9, the amplitude of the high-Q mode falls with increasing feedback gain as the theoretical model predicts, indicating that the sensing transducer is orthogonal to the feedback loop.

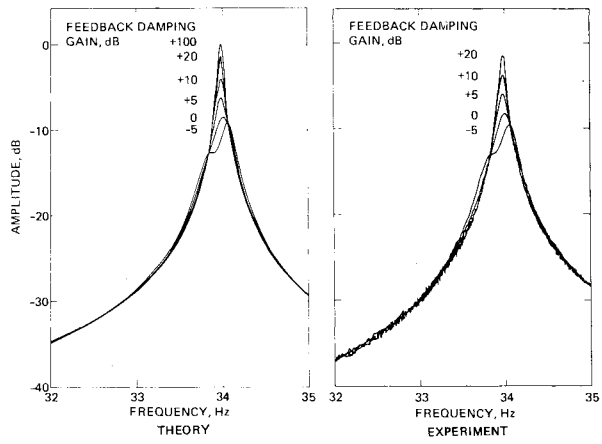

Fig. 8 Amplitude of modes in *j-l* direction with increasing feedback damping gain in *i-k* direction—high damping levels.

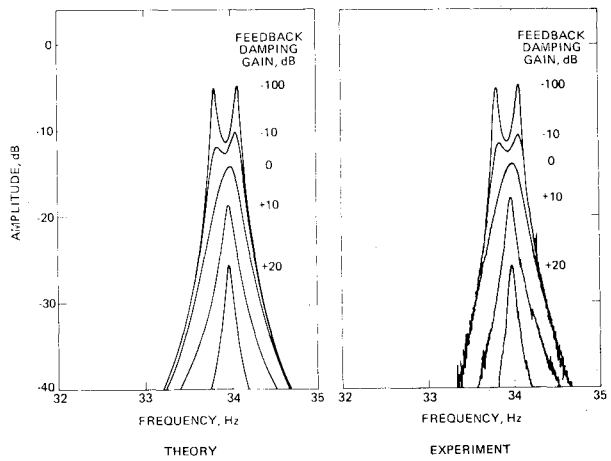

Fig. 9 Amplitude of modes in *i-k* direction with increasing feedback damping gain in *i-k* direction.

Double Feedback Damping Loop Analysis

When both feedback damping loops are operational and orthogonal to each other, both modes are damped equally. Figure 10 shows the motion of the two poles and the zero under increasing feedback gain. At a feedback gain of -20 dB, both the poles and the zero are starting to move off in the complex plane toward the region of higher damping. As the gain increases, they continue to move, accelerating rapidly but maintaining their frequency and relative orientation. Unlike the single-damping-loop cases, there is no return of one of the poles to a low damping point.

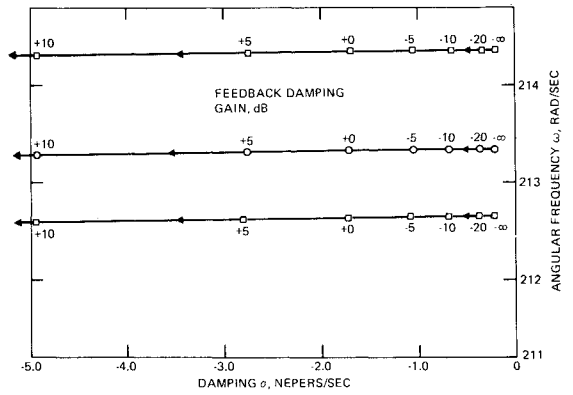

Fig. 10 Motion of poles (□) and zero (○) with increasing gain in both feedback damping loops—expanded view near mode resonances.

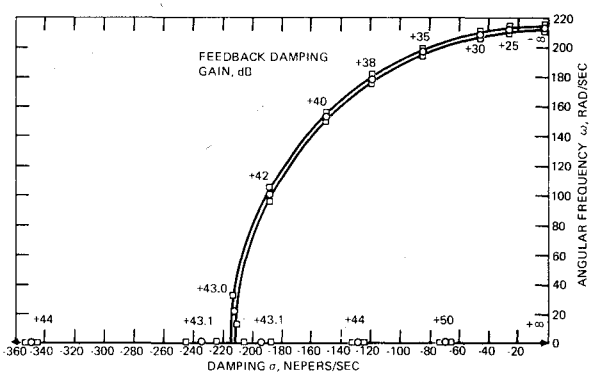

Fig. 11 Motion of poles and zero with increasing gain in both feedback loops.

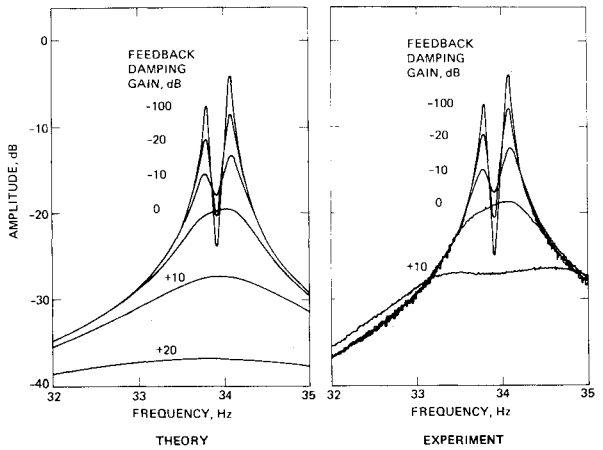

Fig. 12 Amplitude of modes in *j-l* direction with increasing feedback gain in both loops.

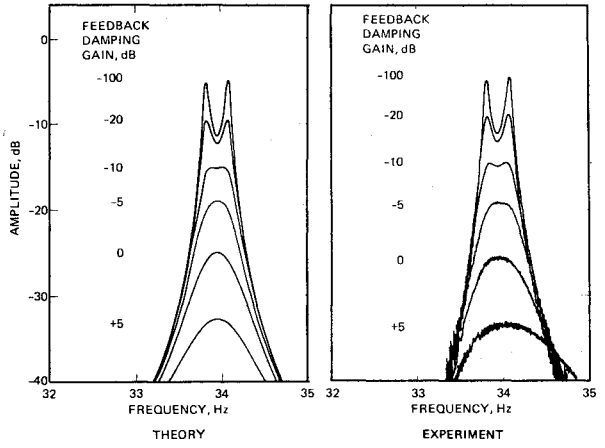

Fig. 13 Amplitude of modes in *i-k* direction with increasing feedback damping gain in both loops.

As the feedback gain is increased still further, the poles and the zeros move in large concentric circles with their center at the origin. As Fig. 11 shows, the inner pole moves a little faster than the zero, and the zero moves faster than the higher-frequency pole, so that the low-frequency pole reaches the real axis before the zero and the other pole. However, as they reach the real axis, the motion reaches its highest "velocity," and it only takes 0.1 dB in feedback damping gain (from 43.0 dB to 43.1 dB) for all three points to go from the complex domain to the real axis, where they meet their counterparts coming up from the lower half of the plane. Again, one set of points moves out along the real axis, getting closer and closer together as they move, while the other set moves in toward the origin, where they all meet at infinite feedback gain.

The effect of the two orthogonal feedback damping loops on the amplitude of the two modes is dramatic. As shown in Fig. 12, the amplitude of the modes as sensed in the direction of the driving transducer array rapidly drops with increasing gain, while the zero smooths out. At 0 dB, we have a smooth hump that is down 14 dB in amplitude, and as the gain increases further, the modes essentially disappear. Again, the theoretical model follows the experimental data well until we get to high gains, where the finite bandwidth of the feedback damping loop in the experimental setup produces spurious bumps and skirts.

As is shown in Fig. 13, which is the response in the direction orthogonal to the driver transducer array, we also find that the modes rapidly and equally damp out when viewed from this direction. The decrease in amplitude is faster here because the modes are 180 deg out of phase for the sensing transducer in this orientation. The more they are damped, the more they overlap and cancel each other out. The agreement of theory with experiment is better in this case because the damped mode is staying within the bandwidth of the feedback damping loop, and so there is a better match between the theoretical model and the real experimental situation.

Conclusion

We have developed a theoretical model that describes the effect of electronic damping applied to the first two orthogonal bending modes of a cylindrical mast. The analytical model predicts that with only one damping circuit active and with low levels of feedback, both modes will be weakly damped. As the amount of feedback gain is increased, however, the original modes recombine into two new modes. One of these new modes is in the direction of the damping loop and is highly damped; the other rotates until it is orthogonal to the damping loop and returns to its original Q. With two orthogonal electronic damping circuits operating, both modes can be strongly damped. The theoretical prediction of the model agrees in detail with the experimental results reported in a previous paper by the authors.

Acknowledgments

The authors wish to acknowledge the role of Dr. A. Jay Palmer in the initial development of this analysis, and for first pointing out the existence of the "rotation" of the modes under increased damping and the existence of a high Q, undamped mode in a direction orthogonal to a single electronic damping loop.

References

[1]Forward, R.L., "Electronic Damping of Orthogonal Bending Modes in a Cylindrical Mast—Experimental," *Journal of Spacecraft and Rockets*, Vol. 18, Jan. 1981, pp. 000-000

[2]Morse, P.M. and Ingard, K.U., *Theoretical Acoustics*, McGraw-Hill, New York, 1968, p. 181.